Structure

Disease-linked mutations cause exposure of a protein quality control degron

Graphical abstract

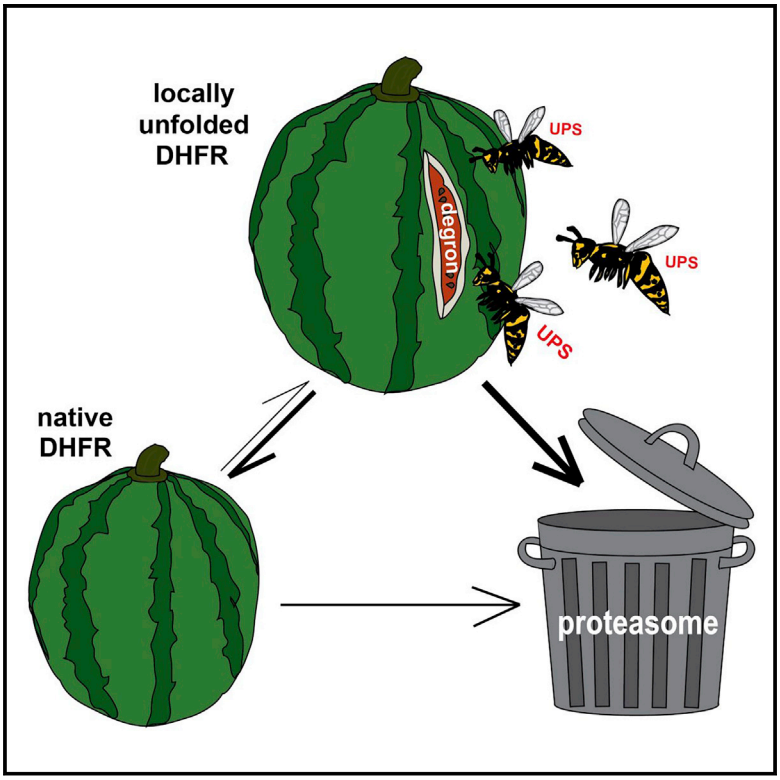

Highlights

- DHFR missense variants are structural destabilized proteasome targets
- Chaperone-dependent and -independent degrons are embedded within the DHFR protein
- The disease-linked DHFR protein variants transiently expose a degron region

Authors

Caroline Kampmeyer, Sven Larsen-Ledet, Morten Rose Wagnkilde, ..., Kaare Teilum, Kresten Lindorff-Larsen, Rasmus Hartmann-Petersen

Correspondence

amelie.stein@bio.ku.dk (A.S.), kaare.teilum@bio.ku.dk (K.T.), lindorff@bio.ku.dk (K.L.-L.), rhpetersen@bio.ku.dk (R.H.-P.)

In brief

Kampmeyer et al. report that disease-linked DHFR missense variants are structurally destabilized and targeted by the protein quality control system for proteasomal degradation. Systematic mapping revealed both chaperone-dependent and -independent degrons are embedded within DHFR. NMR studies revealed that the disease-linked DHFR protein variants transiently expose a degron region.

Kampmeyer et al., 2022, Structure *30*, 1–9
September 1, 2022
https://doi.org/10.1016/j.str.2022.05.016

Please cite this article in press as: Kampmeyer et al., Disease-linked mutations cause exposure of a protein quality control degron, Structure (2022), https://doi.org/10.1016/j.str.2022.05.016

Structure

CellPress

Article

Disease-linked mutations cause exposure of a protein quality control degron

Caroline Kampmeyer,[1] Sven Larsen-Ledet,[1] Morten Rose Wagnkilde,[1] Mathias Michelsen,[1] Henriette K.M. Iversen,[1] Sofie V. Nielsen,[1] Søren Lindemose,[1] Alberto Caregnato,[1] Tommer Ravid,[2] Amelie Stein,[1,*] Kaare Teilum,[1,*] Kresten Lindorff-Larsen,[1,*] and Rasmus Hartmann-Petersen[1,3,*]

[1]The Linderstrøm-Lang Centre for Protein Science, Department of Biology, University of Copenhagen, Ole Maaløes Vej 5, 2200 Copenhagen, Denmark

[2]Department of Biological Chemistry, The Alexander Silberman Institute of Life Sciences, The Hebrew University of Jerusalem, Edmond J. Safra Campus, Givat-Ram, 91904 Jerusalem, Israel

[3]Lead contact

*Correspondence: amelie.stein@bio.ku.dk (A.S.), kaare.teilum@bio.ku.dk (K.T.), lindorff@bio.ku.dk (K.L.-L.), rhpetersen@bio.ku.dk (R.H.-P.)

https://doi.org/10.1016/j.str.2022.05.016

SUMMARY

More than half of disease-causing missense variants are thought to lead to protein degradation, but the molecular mechanism of how these variants are recognized by the cell remains enigmatic. Degrons are stretches of amino acids that help mediate recognition by E3 ligases and thus confer protein degradation via the ubiquitin-proteasome system. While degrons that mediate controlled degradation of, for example, signaling components and cell-cycle regulators are well described, so-called protein-quality-control degrons that mediate the degradation of destabilized proteins are poorly understood. Here, we show that disease-linked dihydrofolate reductase (DHFR) missense variants are structurally destabilized and chaperone-dependent proteasome targets. We find two regions in DHFR that act as degrons, and the proteasomal turnover of one of these was dependent on the molecular chaperone Hsp70. Structural analyses by nuclear magnetic resonance (NMR) and hydrogen/deuterium exchange revealed that this degron is buried in wild-type DHFR but becomes transiently exposed in the disease-linked missense variants.

INTRODUCTION

Since evolution has not selected for overly stable proteins, most proteins are only marginally stable under physiological conditions (Bartlett and Radford, 2009; Kim et al., 2013; Maxwell et al., 2005). Consequently, as a result of mutations or stress conditions, proteins are prone to become structurally destabilized or misfolded (Matreyek et al., 2018; Stein et al., 2019). Since such proteins may interact non-specifically with other cell components and be toxic, all cells are equipped with an effective protein quality control (PQC) system that upholds proteostasis by catalyzing the refolding or degradation of aberrant proteins (Balch et al., 2008; Clausen et al., 2019; Hartl et al., 2011). During translation, Hsp70 and other molecular chaperones promote the folding of nascent proteins but also assist with the refolding of proteins that become damaged after synthesis (Hartl and Hayer-Hartl, 2009). Conversely, degradative PQC typically relies on the ubiquitin-proteasome system (UPS) to eradicate non-native proteins from the intracellular space (Clausen et al., 2019; Enam et al., 2018). Here, often assisted by molecular chaperones, non-native proteins are conjugated to ubiquitin chains by E3 ubiquitin-protein ligases and targeted to the 26S proteasome for degradation.

Virtually all proteins may become structurally destabilized, and recent estimates based on deep-mutational-scanning experiments and computational predictions have shown that more than half of disease-linked loss-of-function missense variants lead to protein degradation, which in turn results in decreased cellular abundance (Cagiada et al., 2021; Yin and Moult, 2019). The PQC system must therefore have a wide-ranging substrate specificity to ensure that any destabilized protein can be recognized while still safeguarding that native proteins are not targeted. Despite several efforts (Geffen et al., 2016; Maurer et al., 2016; Rosenbaum et al., 2011; van der Lee et al., 2014), the discerning features in a destabilized protein, the so-called PQC degrons (Ravid and Hochstrasser, 2008) that are recognized by E3s and thus trigger degradation, still remain rather enigmatic. These degrons are, however, expected to include hydrophobic areas that are buried in the native protein but become exposed upon misfolding (Ravid and Hochstrasser, 2008). Accordingly, recent data have shown that many PQC degrons are hydrophobic and are depleted in negatively charged residues (Mashahreh et al., 2022; Johansson et al., 2022).

To further unravel the nature of the PQC system, we investigated the degradation of human dihydrofolate reductase (DHFR), a known PQC target in *Escherichia coli* (Bershtein et al., 2013; Thompson et al., 2020) and where certain germline missense variants have been linked to recessive megaloblastic anemia (Banka et al., 2011; Cario et al., 2011). We show that

Please cite this article in press as: Kampmeyer et al., Disease-linked mutations cause exposure of a protein quality control degron, Structure (2022), https://doi.org/10.1016/j.str.2022.05.016

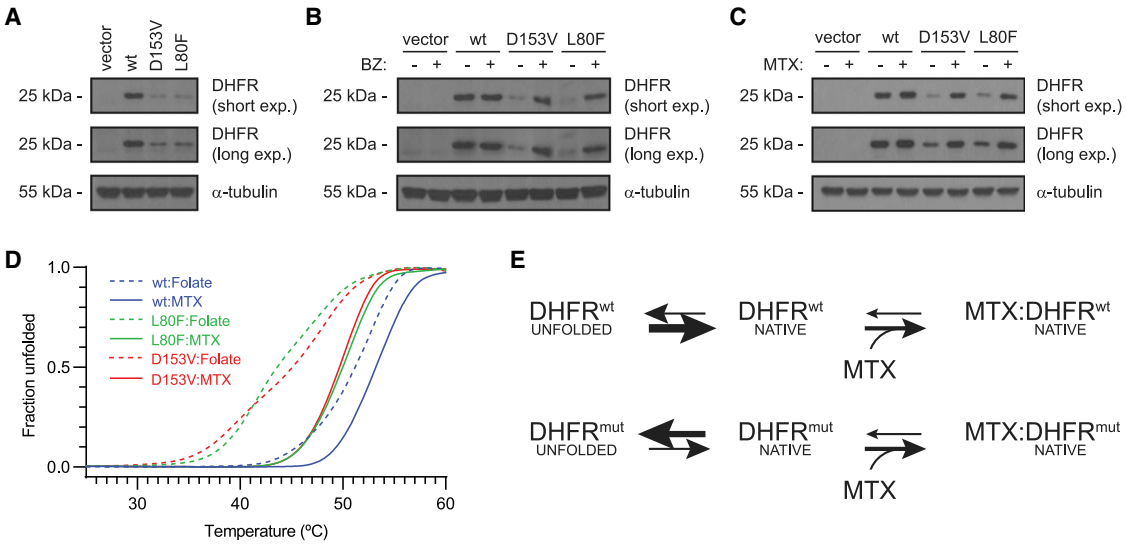

Figure 1. The disease-linked DHFR variants are unstable proteasome targets

(A) The steady-state levels of the DHFR variants in wild-type cells were compared by SDS-PAGE and western blotting using antibodies to DHFR. α-tubulin served as a loading control.

(B) Wild-type cells transformed to express the indicated DHFR variants were grown with (+) or without (-) the proteasome inhibitor bortezomib (BZ), and cell lysates were compared by SDS-PAGE and western blotting using antibodies to DHFR. α-tubulin served as a loading control.

(C) Wild-type cells transformed to express the indicated DHFR variants were grown with (+) or without (-) the DHFR inhibitor methotrexate (MTX), and cell lysates were compared by SDS-PAGE and western blotting using antibodies to DHFR. α-tubulin served as a loading control.

(D) Heat denaturation of DHFR variants with either folate or MTX bound. The unfolding was followed by intrinsic Trp fluorescence at 350 nm, and the signal normalized to give the fraction of unfolded protein.

(E) Model of the stability of wild-type (wt) DHFR and DHFR carrying the L80F or D153V missense mutations (mut) and the effect of MTX binding.

See also Figure S1.

the disease-linked missense variants structurally destabilize the DHFR protein, which in turn is degraded by the UPS. We identified two DHFR regions, DHFR-Deg13-36 and DHFR-Deg61-84 (abbreviated Deg1 and Deg2, respectively), which display degron properties, and find that Deg2 degradation requires Hsp70. Deg2 is positioned in a buried region of DHFR, but hydrogen-deuterium (H/D) exchange studies revealed that the backbone amide hydrogens of Deg2 are more prone to exchange with solvent hydrogens in the disease-linked DHFR than in the wild type, suggesting that it operates to trigger degradation upon partial unfolding.

RESULTS

Disease-linked DHFR missense variants are structurally destabilized and rapidly degraded

Clinical genetics studies have shown that two *DHFR* missense variants (L80F and D153V) are linked to megaloblastic anemia (OMIM: 613839) (Banka et al., 2011; Cario et al., 2011). In both cases the authors found that the protein variants displayed reduced steady-state levels (Banka et al., 2011; Cario et al., 2011), suggesting that the proteins are PQC targets. To test this in a genetically tractable model organism, we expressed wild-type human DHFR and the two disease-linked variants in yeast cells and compared protein levels by western blotting. As expected, both L80F and D153V were present at reduced levels compared with wild-type DHFR (Figure 1A). This reduction was caused by proteasomal degradation since the protein levels were, in both cases, restored when the proteasome was blocked by bortezomib (BZ) (Figure 1B). This suggests that the disease-linked DHFR proteins are structurally destabilized PQC targets. However, since addition of the DHFR inhibitor methotrexate (MTX) also led to a stabilization of the DHFR variants (Figure 1C), the structural destabilization is not so severe that the DHFR variants are unable to bind MTX. Accordingly, both variants were soluble cytosolic proteins (Figure S1A), adept at binding an MTX resin (Figure S1B), and conferred MTX resistance to the yeast cells when overexpressed, albeit not to same extent as wild-type DHFR (Figure S1C). This indicates that the disease-linked DHFR variants are hypomorphs, i.e., destabilized variants that retain some, but not full, function.

In agreement with the cellular studies, we found that both purified DHFR variants in their folate-bound states displayed at least 6°C reduction in the unfolding midpoint from the heat-denaturation experiment compared with folate-bound wild-type DHFR (Figure 1D). The temperature unfolding midpoints are 43.5°C and 45.1°C for L80F and D153V, respectively, compared with 51.1°C for wild-type DHFR. These results indicate a sizable change in stability, and we note that while the unfolding is not reversible, a change in melting temperature of this magnitude would correspond roughly to a decrease in thermodynamic stability of 12–16 kJ/mol (Watson et al., 2018). We also note that the temperature unfolding curves in the presence of folate are rather shallow and that around 10% of the protein is already unfolded at 37°C for the variants. When DHFR is bound to MTX, there is a clear increase in the unfolding

Please cite this article in press as: Kampmeyer et al., Disease-linked mutations cause exposure of a protein quality control degron, Structure (2022), https://doi.org/10.1016/j.str.2022.05.016

CellPress

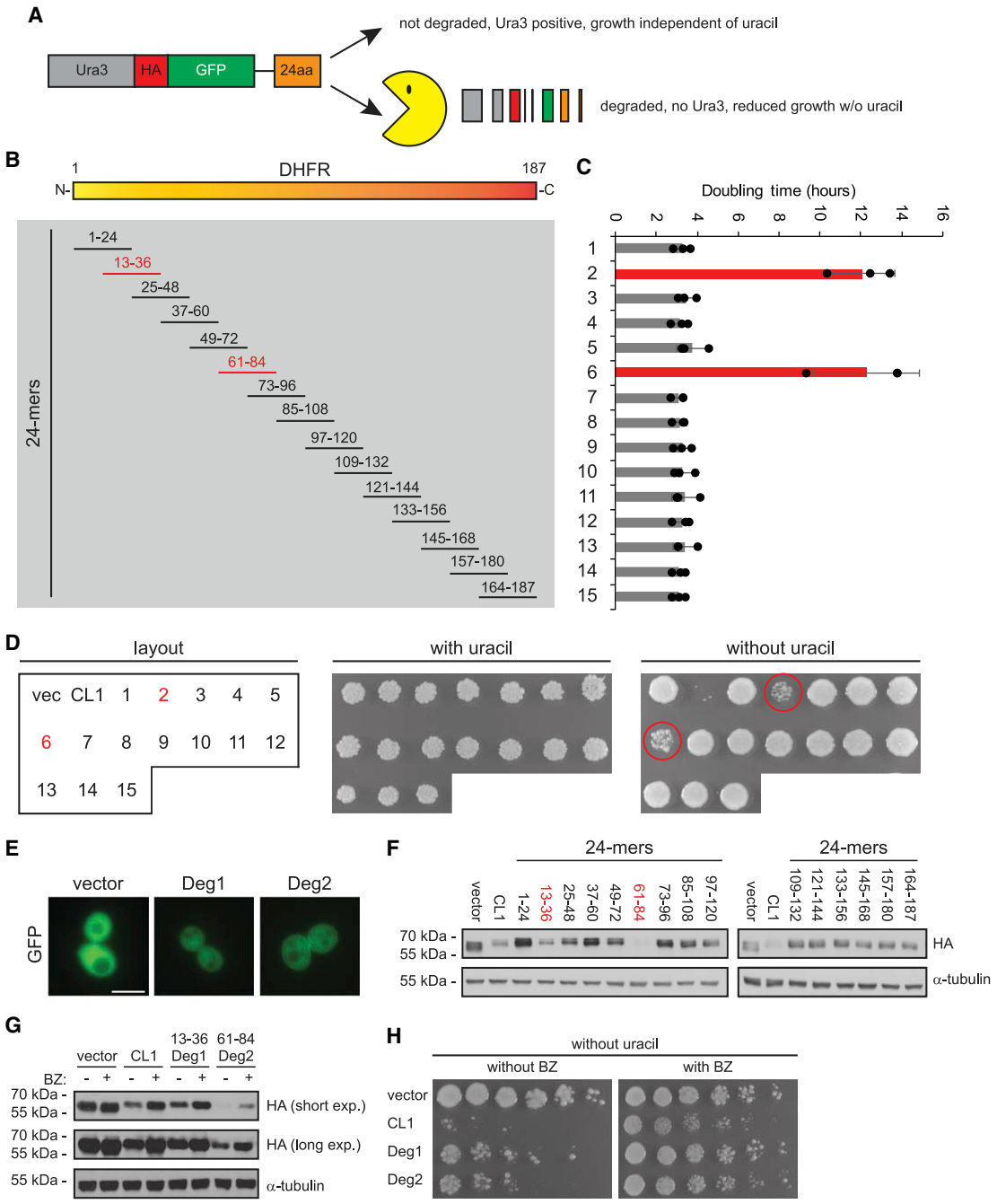

Figure 2. Fragments of the human DHFR protein display degron activity

(A) In the yeast-selection system used for identifying degrons, the different 24-residue DHFR fragments are fused after a linker to the C terminus of a Ura3-HA-GFP fusion protein. In case a fragment acts as a degron, the entire fusion protein will be degraded, and the cells will be unable to grow without the addition of uracil to the medium.

(B) The 187-residue human DHFR protein (yellow/orange bar) was divided into the indicated 15 different 24-residue partially overlapping fragments (24-mers) and fused to the C terminus of the Ura3 reporter.

(C) Growth was monitored in medium lacking uracil, and the doubling times were determined. Two fragments (red) led to strongly reduced growth (increased doubling times). The error bars indicate the standard deviation (n = 3).

(D) The growth of yeast cells containing the indicated fragments (left panel and B) was monitored by spotting an equal amount of culture onto solid media with (middle panel) or without (right panel) uracil. Note that the fragments displaying increased doubling times in (C) also grow poorly on solid medium without uracil (circled). The vector and CL1 fusion protein were included as controls.

(E) Cells carrying the indicated expression constructs were analyzed by fluorescence microscopy. The Deg1 and Deg2 fusion proteins are cytosolic and present in reduced amounts compared with the vector control. Bar: 5 μm.

(legend continued on next page)

Please cite this article in press as: Kampmeyer et al., Disease-linked mutations cause exposure of a protein quality control degron, Structure (2022), https://doi.org/10.1016/j.str.2022.05.016

temperature of both wild type and the variants. The two variants are only destabilized by approximately 3°C in the presence of MTX, and the unfolding curves become steeper than those recorded in the presence of folate. Thus, the disease-causing mutations significantly destabilize the folded structure of DHFR, but in agreement with previous studies (Hingorani et al., 2017), the destabilization may be alleviated by binding of ligands (Figure 1E). Indeed, we were unable to purify the DHFR variants in the ligand-free apo state. Therefore, together, these results show that the mutation-induced structural destabilization leads to proteasomal degradation of the disease variants.

Systematic screen for PQC degrons in DHFR

Since the above data show that the disease-linked DHFR protein variants are proteasome targets, we proceeded to map potential degrons in DHFR using a yeast-selection system (Geffen et al., 2016) where potential degrons are fused in frame downstream of a Ura3-HA-GFP fusion protein (Figure 2A). Thus, in case a fragment containing a degron is fused to the reporter, the processive nature of proteasomal degradation ensures that the entire fusion protein is degraded, and cells carrying a deletion in *ura3* should therefore not be able to grow unless the medium is supplemented with uracil (Figure 2A).

The 187-residue full-length DHFR protein was divided into 15 different, partially overlapping 24-residue fragments and produced in frame with the Ura3-reporter (Figures 2A and 2B). The artificial 16-residue CL1 peptide that is a known degron (Gilon et al., 1998, 2000; Metzger et al., 2008; Ravid et al., 2006) was included as a control. The length of 24 residues was selected since we reasoned that fragments of this size are likely sufficiently long to contain degradation signals but too short to harbor significant structure. The different fragments containing potential degrons will therefore most likely be present as exposed linear segments in this construct. The growth of most strains was unaffected by the C-terminal fusions (Figures 2B and 2C), suggesting that these fragments do not contain degrons. However, fragments composed of DHFR residues 13–36 and 61–84 led to significantly reduced growth in both liquid growth assays (Figure 2C) and on solid medium (Figure 2D). From here on, we will refer to the 13–36 fragment as Deg1 and the 61–84 fragment as Deg2.

Fluorescence microscopy revealed that the Deg1 and Deg2 fusions were cytosolic (Figure 2E). However, in agreement with the degrons leading to reduced cellular amounts of the reporter protein, fusion of the degrons to the reporter led to clearly reduced GFP intensities (Figure 2E). Albeit there was some variation in the steady-state levels of multiple fragments, Deg1 and Deg2 fusions were clearly found at reduced levels in western blots of whole-cell lysates (Figure 2F). The reduced amount of the degron fusion proteins was caused by proteasomal degradation, since adding sublethal amounts of BZ led to increased amounts of the reporter proteins (Figure 2G), and also restored cell growth in the absence of uracil (Figure 2H).

To examine which properties of the peptides caused them to be degrons, we generated Deg1 and Deg2 variants where all hydrophobic residues were exchanged with alanine (Φ0). As expected, this eliminated degron function (Figures S2A–S2C), highlighting the fact that the PQC recognizes exposed hydrophobic residues. In contrast, substituting all lysine residues with arginine (KallR) did not cause the peptides to lose the ability to act as degrons (Figures S2A–S2C), suggesting that ubiquitylation occurs in the Ura3-GFP fusion partner. Finally, since Deg2 includes the L80 residue, we tested the effect of an L80F variant in the Deg2 context. This substitution, which has a destabilizing effect in the DHFR full-length context, does not appear to affect the degron activity of Deg2 itself (Figures S2A–S2C).

Considering that relevant PQC degrons should be exclusively found in buried regions, we mapped the position of Deg1 and Deg2 on the DHFR structure (PDB: 1U72) (Cody et al., 2005). Both degrons contained exposed and buried parts (Figures 3A and 3B). However, when, as a measure of exposure, we mapped the number of C-beta neighbors (C-alpha for glycine) within 8 Å of each residue (Yuan, 2005), the central region of Deg2 clearly contained a buried stretch of residues (Figure 3C; Table S1). To probe these sequences further, we generated a number of N- and C-terminal truncations of Deg2 (Figure 3D) and tested their degron activity as before (Figures 3E and 3F). Growth assays revealed a minimum 8-amino-acid-residue sequence (RINLVLSR) that was required for degron activity and led to reduced levels of the reporter protein (Figures 3E and 3F). We noted that in western blots, the Deg2Δ12 appeared more abundant than the Deg2 24-mer. However, the Deg2Δ16 was still destabilizing (Figures 3E and 3F), suggesting that the central 8-residue degron motif is affected by the neighboring sequence context, which potentially could affect binding and/or exposure. We note that this central Deg2 region bears some resemblance to the preferred Hsp70-binding sequence consisting of hydrophobic residues flanked by positive charges (Rudiger et al., 1997), and indeed, a recent study indicates that Hsp70 binding sites can act as degrons (Abildgaard et al., 2021). We therefore proceeded to test if the degron activity required Hsp70. In the case of Deg1, we only observed very slight effects (Figures 3G and S2D), but for Deg2, the degron activity was clearly dependent on the Hsp70 paralogues Ssa1 and Ssa2 (Figures 3G and S2D). This suggests that Deg2 indeed represents a PQC degron that, upon exposure, targets proteins for chaperone-assisted proteasomal degradation. In agreement with this, the stability of the full-length DHFR variants was also increased in mutants lacking Ssa1 or Ssa2 (Figure S2E).

H/D-exchange NMR

To test if the identified degron regions in DHFR were relevant in context of the full-length DHFR protein and disease-linked protein variants, we next decided to measure the local structural

(F) The steady-state levels of cells carrying the indicated expression constructs were analyzed by SDS-PAGE and western blotting using antibodies to the hemagglutinin (HA) tag on the reporter protein. α-tubulin served as a loading control.
(G) The vector, CL1, Deg1, and Deg2 strains were grown with (+) or without (-) the proteasome inhibitor BZ, and whole-cell lysates were compared by SDS-PAGE and western blotting using antibodies to the HA tag on the reporter fusion. α-tubulin served as a loading control.
(H) Growth was compared on solid medium without uracil and with or without BZ by spotting serial dilutions of the indicated cultures.
See also Figure S2.

Please cite this article in press as: Kampmeyer et al., Disease-linked mutations cause exposure of a protein quality control degron, Structure (2022), https://doi.org/10.1016/j.str.2022.05.016

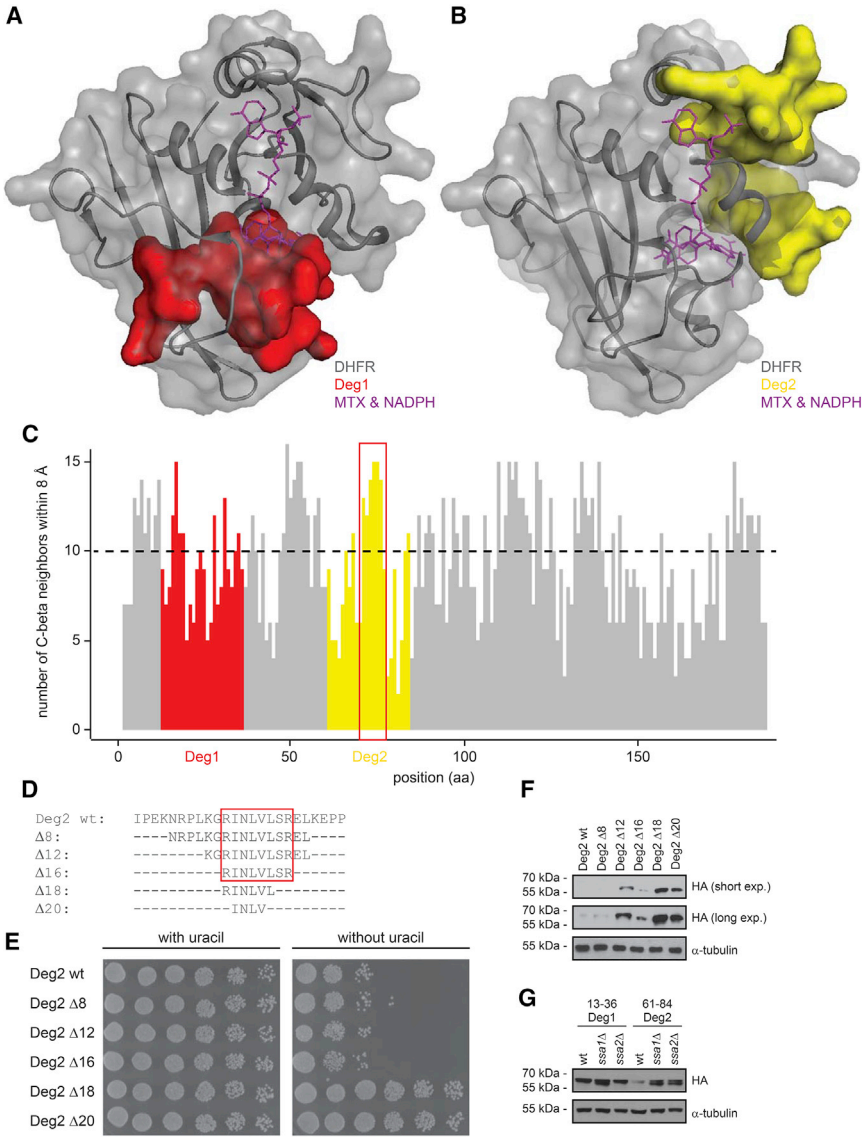

Figure 3. Positioning of Deg1 and Deg2 in DHFR

(A) The position of Deg1 in the DHFR structure (PDB: 1U72). Deg1 is marked in red. The inhibitor and substrate MTX and NADPH, respectively, are shown in purple.

(B) The position of Deg2 in the DHFR structure. Deg2 is marked in yellow, while MTX and NADPH are purple.

(C) The number of C-beta neighbors for each residue in DHFR is shown. Deg1 is shown in red. Deg2 is shown in yellow. The dashed line marks a threshold of 10 neighbors. Note that a high value indicates that the residue is buried. The red box marks the central buried part of Deg2.

(D) The amino-acid sequence of the tested truncations of the Deg2 fragment. The minimal degron region is boxed.

(E) The growth of cells carrying the indicated Deg2 truncations was compared by spotting serial dilutions of the cultures on solid medium with or without uracil.

(F) The steady-state amounts of the indicated Deg2 variants were compared by SDS-PAGE and western blotting of whole-cell extracts using antibodies to the HA tag. α-tubulin served as a loading control.

(G) The steady-state amounts of the Deg1 and Deg2 fusion proteins in WT, *ssa1*Δ, and *ssa2*Δ cells were compared by SDS-PAGE and western blotting of cell extracts using antibodies to the HA tag. α-tubulin served as a loading control.

See also Figure S2.

stabilities by H/D exchange of the backbone amides by nuclear magnetic resonance (NMR) spectroscopy. The chemical shift of Cα is a sensitive probe of structural change. We therefore compared the Cα chemical shifts of the two variants to those of wild-type (WT) DHFR and found that the structures of the DHFR variants overall are the same as for the WT, with some local differences around the mutation sites (Figure S3A). At the first time point in the hydrogen-exchange time series, recorded approximately 5 min after the lyophilized protein was dissolved in D_2O, we observed peaks from 130, 123, and 126 of the 174 non-proline backbone amides in WT, L80F, and D153V, respectively (Figure 4A). Within the 5,352 min (3.7 days) for which the hydrogen exchange was followed, we could quantify the exchange kinetics for most of the observed amide residues. For some residues, the exchange was either too slow or too fast to be quantified (Figure S3B). We thus quantified the change in the exchange rates for 101 and 102 of the amides in L80F and D153V relative to the WT (Figure 4B). Most amides exchange faster in the two variants, although in both variants, a few also exchanged slower. These slower-exchanging residues are probably a result of subtle structural changes induced by the mutations that stabilize isolated hydrogen bonds. In L80F, we observe faster exchange kinetics mostly between residue 51 and 126, which corresponds to the residues in the vicinity of position 80. The L80F mutation thus results in local destabilization of the hydrogen bonds, including those involving the amides in Deg2 (Figure 4C). However, L80F appears to leave the local stability of the Deg1 region unaffected. D153V on the other hand has a more global effect on the exchange rates and affects residues throughout the structure, including Deg2 (Figure 4C), and the hydrogen bonds in both Deg1 and Deg2 are weakened. The increase in the exchange rates for both variants are between 2^1 and 2^4, which corresponds to an amide in the variants on average spends 2 to 16 times more time in the open state than the same amide in WT does. This estimate assumes that the exchange process follows the EX2 limiting case of the Linderstrøm-Lang model for hydrogen exchange that dominates at neutral and low pH (Hvidt and Nielsen, 1966). In conclusion, our H/D-exchange data show that the disease-linked DHFR variants more frequently visit a locally unfolded state where the hydrogen bonds in the 8-residue segment comprising Deg2 are broken.

Please cite this article in press as: Kampmeyer et al., Disease-linked mutations cause exposure of a protein quality control degron, Structure (2022), https://doi.org/10.1016/j.str.2022.05.016

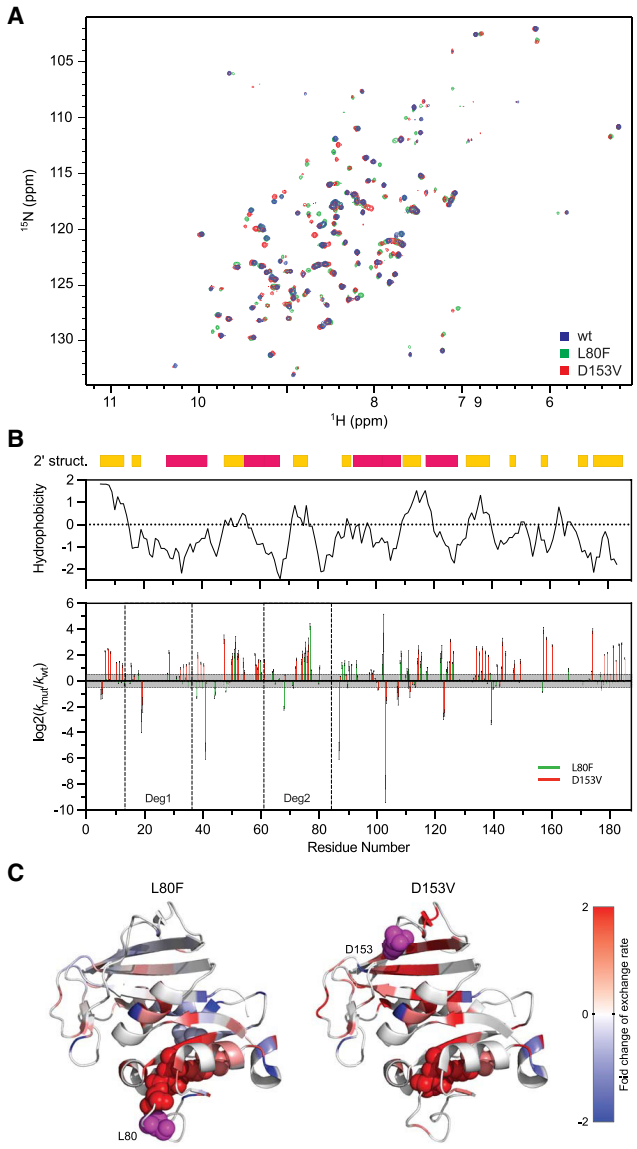

Figure 4. Local stability change in DHFR variants from hydrogen-deuterium exchange

(A) ^{15}N-heteronuclear single quantum coherence (HSQC) spectrum from the hydrogen-deuterium exchange (HDX) series of WT (blue), L80F (green), and D153V (red).

(B) Bottom: residue-specific change in the measured hydrogen exchange rate, k_{mut}, for the two mutants relative to the exchange rate for the WT, k_{wt}. Log base 2 of the ratio is plotted and shows how many times the hydrogen-exchange rates of the mutants have doubled relative to the WT. Middle: the hydrophobicity was calculated from the Kyte and Doolittle scale with a moving average of nine residues. Top: the secondary structure is shown as red and yellow boxes indicating α helix and β strand, respectively.

(C) The values in (B) plotted on the crystal structure of DHFR with a color scale from blue (-2) to red (2). The mut sites are shown as magenta spheres. The residues of Deg2 for which we have HDX information are also shown as spheres color coded as the rest of the structure.

See also Figure S3.

Finally, we sought to examine if mutations within Deg2, which we designed to disrupt the degron activity, would lead to a stabilization of the L80F DHFR variant. As the central part of Deg2 is deeply buried, we analyzed the steady-state levels of L80F variants with additional mutations at positions K69 and R78 that are partially exposed and therefore might not be critical for DHFR structural stability. Since it was recently shown that negative charges disrupt PQC degron activity (Mashahreh et al., 2022; Johansson et al., 2022), we tested the K69E and R78E substitutions in the DHFR L80F protein. We also included a mutation in the buried Deg2 region at position N73 (N73A). However, in all cases, the DHFR variants were expressed at levels as low or lower than the L80F single mutant (Figure S3C), indicating that in this case, it is not possible to locally disrupt Deg2 without globally affecting DHFR stability.

DISCUSSION

Currently, it is well established that certain missense mutations may cause protein destabilization and degradation (Stein et al., 2019) and that this is the underlying molecular mechanism for a number of hereditary diseases, including cystic fibrosis, phenylketonuria, and various cancer predisposition disorders (Abildgaard et al., 2019; Ahner et al., 2007; Arlow et al., 2013; Canaff et al., 2012; Clausen et al., 2020; Gersing et al., 2021; Pey et al., 2007; Scheller et al., 2019). Here, we add hereditary megaloblastic anemia, linked to germline *DHFR* variants, to this list. Our results reveal that both DHFR protein variants are PQC targets that are structurally destabilized and degraded. However, upon binding MTX, the proteins are significantly stabilized and no longer PQC targets. This suggests that the DHFR variants are not strongly misfolded and still adept at binding MTX. These observations are in line with previous experiments using a destabilized, aggregation-prone variant of *E. coli* DHFR, which showed that this variant could be stabilized inside *E. coli* by the addition of the DHFR ligand trimethoprim (Hingorani et al., 2017). In the case of the L80F and D153V variants of human DHFR, we speculate that they are likely to be partially functional, given that *DHFR* is an essential gene, and disease-linked *DHFR* variants are thus bound to be hypomorph rather than null alleles.

Although several regions of DHFR become more dynamic in the disease variants, one region in particular is exposed in both disease-linked proteins and overlaps with a mapped degron region, namely an 8-residue (RINLVLSR) buried fragment from positions 71–78. Interestingly, the same region appears to be important for Lon-catalyzed degradation of DHFR in *E. coli* (Thompson et al., 2020), which also agrees with the specificity of Lon for buried hydrophobic regions (Gur and Sauer, 2008). Recent studies have defined a number of new degrons in human cells (Koren et al., 2018; Timms et al., 2019), but we do not know if the ones identified here also function in human cells. However, as the PQC system is highly conserved, the same rules for degron recognition likely apply in all eukaryotes. We observed that the Deg2 region requires Hsp70 for degradation, while the other identified degron appears to function independently of Hsp70. This suggests that upon the mutation-induced structural destabilization, there is increased transient exposure of Deg2, which in turn leads to chaperone-dependent proteasomal degradation of the DHFR variants. It is thus possible that inhibition of Hsp70 would lead to increased function of the DHFR variants so that chaperones, similar to the situation of with Lon in bacteria (Thompson et al., 2020), could shape the

genotype-phenotype landscape of DHFR in yeast cells. This is in agreement with a number of other studies that have linked molecular chaperones with the UPS (Gowda et al., 2013; Kampmeyer et al., 2017; Kandasamy and Andreasson, 2018; Kriegenburg et al., 2014; Mathiassen et al., 2015; Samant et al., 2018), including as E3 co-factors involved in substrate selection (Murata et al., 2001; Qian et al., 2006; Xu et al., 2002) or as carriers of misfolded proteins to E3 ligases (Comyn et al., 2016; Guerriero et al., 2013; Shiber and Ravid, 2014). For instance, the human E3 ligase CHIP associates directly with Hsp90 and Hsp70 to catalyze the ubiquitylation of chaperone-bound clients (Connell et al., 2001; Demand et al., 2001). We thus propose that Deg2 functions as a classical PQC degron, in that it is buried in WT DHFR, but becomes exposed and elicits chaperone-dependent degradation in the destabilized disease-linked DHFR variants. However, we were unable to show this directly, since there were no stabilizing effects of introducing mutations aimed at destroying Deg2 in context of full-length DHFR. Although it has recently been shown that negative charges disrupt PQC-degron activity (Mashahreh et al., 2022; Johansson et al., 2022), full-length DHFR L80F carrying either K69E or R78E substitutions was still unstable. As Deg2 is deeply embedded in the DHFR structure, we speculate that the degron-disrupting mutations destabilize DHFR, perhaps resulting in the exposure of Deg1 and/or leading to the formation of new degrons. Thus, although we cannot exclude that the unstable DHFR variants are recognized independently of Deg2, this is the only region that becomes more exposed for both disease-linked variants. In addition, as we do not know to what extent the variants bind folate in the cells, it is also possible that the folate binding to WT DHFR potentially masks a degron. Although we have not analyzed how MTX or other ligands stabilize DHFR, work on bacterial DHFRs suggest that ligand binding has a global effect on hydrogen exchange (Polshakov et al., 2006; Yamamoto et al., 2004) and thus no specific effects on individual degrons.

Based on the NMR data, Deg1 seems less relevant for the disease-linked DHFR variants. Interestingly, compared with Deg2, Deg1 appears more exposed also in native WT DHFR, suggesting that in the native protein, Deg1 is maintained in a conformation that does not trigger degradation. As a 24-mer peptide, however, and presumably in the fully denatured state of DHFR, it would become recognized by an E3. The two DHFR variants that we tested here are currently the only known disease-linked alleles of DHFR. However, it is possible that Deg1 is relevant for other, presently unknown DHFR variants that may become structurally perturbed in a way leading to Deg1 recognition.

In conclusion, the results presented here provide detailed mechanistic insight into the degradation of disease-relevant PQC targets and show an example of how a hydrophobic and buried region in a native protein may become exposed and target the protein for proteasomal degradation.

STAR★METHODS

Detailed methods are provided in the online version of this paper and include the following:

SUPPLEMENTAL INFORMATION

Supplemental information can be found online at https://doi.org/10.1016/j.str.2022.05.016.

ACKNOWLEDGMENTS

The authors thank Anne-Marie Lauridsen for technical assistance and Dr. Michael Askvad Sørensen for assistance with DHFR purification. The present work was funded by the Novo Nordisk Foundation (https://novonordiskfonden.dk) challenge program PRISM (to K.L.-L., A.S., and R.H.-P.), NNF18OC0052441 (to R.H.-P.), and NNF18OC0032996 (to K.T.); the Lundbeck Foundation (https://www.lundbeckfonden.com) R272-2017-452 and R209-2015-3283 (to A.S.); and Danish Council for Independent Research (Det Frie Forskningsråd) (https://dff.dk) 7014-00039B (to R.H.-P.). The funders had no role in study design, data collection and analysis, decision to publish, or preparation of the manuscript.

AUTHOR CONTRIBUTIONS

C.K., M.M., S.L.-L., A.C., M.R.W., S.V.N., S.L., H.K.M.I., and A.S. performed the experiments, C.K., T.R., A.S., K.L.-L., K.T., and R.H.-P. analyzed the data. T.R., K.L.-L., and R.H.-P. conceived the study. C.K. and R.H.-P. wrote the paper.

DECLARATION OF INTERESTS

The authors declare no competing interests.

Received: January 14, 2021
Revised: April 8, 2022
Accepted: May 18, 2022
Published: June 13, 2022

REFERENCES

Abildgaard, A.B., Petersen, S.D., Larsen, F.B., Kampmeyer, C., Johansson, K.E., Stein, A., Ravid, T., Andreasson, C., Jensen, M.K., Lindorff-Larsen, K., and Hartmann-Petersen, R. (2021). HSP70-binding motifs function as protein quality control degrons. Preprint. bioRxiv. https://doi.org/10.1101/2021.12.22.473789.

Abildgaard, A.B., Stein, A., Nielsen, S.V., Schultz-Knudsen, K., Papaleo, E., Shrikhande, A., Hoffmann, E.R., Bernstein, I., Gerdes, A.M., Takahashi, M., et al. (2019). Computational and cellular studies reveal structural destabilization and degradation of MLH1 variants in Lynch syndrome. Elife *8*, e49138. https://doi.org/10.7554/elife.49138.

Ahner, A., Nakatsukasa, K., Zhang, H., Frizzell, R.A., and Brodsky, J.L. (2007). Small heat-shock proteins select ΔF508-CFTR for endoplasmic reticulum-associated degradation. Mol. Biol. Cell *18*, 806–814. https://doi.org/10.1091/mbc.e06-05-0458.

Arlow, T., Scott, K., Wagenseller, A., and Gammie, A. (2013). Proteasome inhibition rescues clinically significant unstable variants of the mismatch repair protein Msh2. Proc. Natl. Acad. Sci. U. S. A *110*, 246–251. https://doi.org/10.1073/pnas.1215510110.

Balch, W.E., Morimoto, R.I., Dillin, A., and Kelly, J.W. (2008). Adapting proteostasis for disease intervention. Science *319*, 916–919. https://doi.org/10.1126/science.1141448.

Banka, S., Blom, H.J., Walter, J., Aziz, M., Urquhart, J., Clouthier, C.M., Rice, G.I., de Brouwer, A.P., Hilton, E., Vassallo, G., et al. (2011). Identification and characterization of an inborn error of metabolism caused by dihydrofolate reductase deficiency. Am. J. Hum. Genet. *88*, 216–225. https://doi.org/10.1016/j.ajhg.2011.01.004.

Bartlett, A.I., and Radford, S.E. (2009). An expanding arsenal of experimental methods yields an explosion of insights into protein folding mechanisms. Nat. Struct. Mol. Biol. *16*, 582–588. https://doi.org/10.1038/nsmb.1592.

Bershtein, S., Mu, W., Serohijos, A.W., Zhou, J., and Shakhnovich, E.I. (2013). Protein quality control acts on folding intermediates to shape the effects of mutations on organismal fitness. Mol. Cell *49*, 133–144. https://doi.org/10.1016/j.molcel.2012.11.004.

Bhabha, G., Ekiert, D.C., Jennewein, M., Zmasek, C.M., Tuttle, L.M., Kroon, G., Dyson, H.J., Godzik, A., Wilson, I.A., and Wright, P.E. (2013). Divergent evolution of protein conformational dynamics in dihydrofolate reductase. Nat. Struct. Mol. Biol. *20*, 1243–1249. https://doi.org/10.1038/nsmb.2676.

Cagiada, M., Johansson, K.E., Valanciute, A., Nielsen, S.V., Hartmann-Petersen, R., Yang, J.J., Fowler, D.M., Stein, A., and Lindorff-Larsen, K. (2021). Understanding the origins of loss of protein function by analyzing the effects of thousands of variants on activity and abundance. Mol. Biol. Evol. *38*, 3235–3246. https://doi.org/10.1093/molbev/msab095.

Canaff, L., Vanbellinghen, J.F., Kanazawa, I., Kwak, H., Garfield, N., Vautour, L., and Hendy, G.N. (2012). Menin missense mutants encoded by the MEN1 gene that are targeted to the proteasome: restoration of expression and activity by CHIP siRNA. J. Clin. Endocrinol. Metab. *97*, E282–E291. https://doi.org/10.1210/jc.2011-0241.

Cario, H., Smith, D.E., Blom, H., Blau, N., Bode, H., Holzmann, K., Pannicke, U., Hopfner, K.P., Rump, E.M., Ayric, Z., et al. (2011). Dihydrofolate reductase deficiency due to a homozygous DHFR mutation causes megaloblastic anemia and cerebral folate deficiency leading to severe neurologic disease. Am. J. Hum. Genet. *88*, 226–231. https://doi.org/10.1016/j.ajhg.2011.01.007.

Clausen, L., Abildgaard, A.B., Gersing, S.K., Stein, A., Lindorff-Larsen, K., and Hartmann-Petersen, R. (2019). Protein stability and degradation in health and disease. Adv. Protein Chem. Struct. Biol. *114*, 61–83. https://doi.org/10.1016/bs.apcsb.2018.09.002.

Clausen, L., Stein, A., Grønbæk-Thygesen, M., Nygaard, L., Søltoft, C.L., Nielsen, S.V., Lisby, M., Ravid, T., Lindorff-Larsen, K., and Hartmann-Petersen, R. (2020). Folliculin variants linked to Birt-Hogg-Dubé syndrome are targeted for proteasomal degradation. PLoS Genet. *16*, e1009187. https://doi.org/10.1371/journal.pgen.1009187.

Cody, V., Luft, J.R., and Pangborn, W. (2005). Understanding the role of Leu22 variants in methotrexate resistance: comparison of wild-type and Leu22Arg variant mouse and human dihydrofolate reductase ternary crystal complexes with methotrexate and NADPH. Acta Crystallogr. D. Biol. Crystallogr. *61*, 147–155. https://doi.org/10.2210/pdb1u71/pdb.

Comyn, S.A., Young, B.P., Loewen, C.J., and Mayor, T. (2016). Prefoldin promotes proteasomal degradation of cytosolic proteins with missense mutations by maintaining substrate solubility. PLoS Genet. *12*, e1006184. https://doi.org/10.1371/journal.pgen.1006184.

Connell, P., Ballinger, C.A., Jiang, J., Wu, Y., Thompson, L.J., Hohfeld, J., and Patterson, C. (2001). The co-chaperone CHIP regulates protein triage decisions mediated by heat-shock proteins. Nat. Cell Biol. *3*, 93–96. https://doi.org/10.1038/35050618.

Cox, J.S., Chapman, R.E., and Walter, P. (1997). The unfolded protein response coordinates the production of endoplasmic reticulum protein and endoplasmic reticulum membrane. Mol. Biol. Cell *8*, 1805–1814. https://doi.org/10.1091/mbc.8.9.1805.

Delaglio, F., Grzesiek, S., Vuister, G.W., Zhu, G., Pfeifer, J., and Bax, A. (1995). NMRPipe: a multidimensional spectral processing system based on UNIX pipes. J. Biomol. NMR *6*, 277–293. https://doi.org/10.1007/bf00197809.

Demand, J., Alberti, S., Patterson, C., and Hohfeld, J. (2001). Cooperation of a ubiquitin domain protein and an E3 ubiquitin ligase during chaperone/proteasome coupling. Curr. Biol. *11*, 1569–1577. https://doi.org/10.1016/s0960-9822(01)00487-0.

Enam, C., Geffen, Y., Ravid, T., and Gardner, R.G. (2018). Protein quality control degradation in the nucleus. Annu. Rev. Biochem. *87*, 725–749. https://doi.org/10.1146/annurev-biochem-062917-012730.

Geffen, Y., Appleboim, A., Gardner, R.G., Friedman, N., Sadeh, R., and Ravid, T. (2016). Mapping the landscape of a eukaryotic degronome. Mol. Cell *63*, 1055–1065. https://doi.org/10.1016/j.molcel.2016.08.005.

Gersing, S.K., Wang, Y., Grønbæk-Thygesen, M., Kampmeyer, C., Clausen, L., Willemoës, M., Andréasson, C., Stein, A., Lindorff-Larsen, K., and Hartmann-Petersen, R. (2021). Mapping the degradation pathway of a disease-linked aspartoacylase variant. PLoS Genet. *17*, e1009539. https://doi.org/10.1371/journal.pgen.1009539.

Gietz, R.D., and Schiestl, R.H. (2007). High-efficiency yeast transformation using the LiAc/SS carrier DNA/PEG method. Nat. Protoc. *2*, 31–34. https://doi.org/10.1038/nprot.2007.13.

Gilon, T., Chomsky, O., and Kulka, R.G. (1998). Degradation signals for ubiquitin system proteolysis in Saccharomyces cerevisiae. EMBO J. *17*, 2759–2766. https://doi.org/10.1093/emboj/17.10.2759.

Gilon, T., Chomsky, O., and Kulka, R.G. (2000). Degradation signals recognized by the Ubc6p-Ubc7p ubiquitin-conjugating enzyme pair. Mol. Cell Biol. *20*, 7214–7219. https://doi.org/10.1128/mcb.20.19.7214-7219.2000.

Gowda, N.K.C., Kandasamy, G., Froehlich, M.S., Dohmen, R.J., and Andreasson, C. (2013). Hsp70 nucleotide exchange factor Fes1 is essential for ubiquitin-dependent degradation of misfolded cytosolic proteins. Proc. Natl. Acad. Sci. U. S. A *110*, 5975–5980. https://doi.org/10.1073/pnas.1216778110.

Guerriero, C.J., Weiberth, K.F., and Brodsky, J.L. (2013). Hsp70 targets a cytoplasmic quality control substrate to the San1p ubiquitin ligase. J. Biol. Chem. *288*, 18506–18520. https://doi.org/10.1074/jbc.m113.475905.

Gur, E., and Sauer, R.T. (2008). Recognition of misfolded proteins by Lon, a AAA(+) protease. Genes Dev. *22*, 2267–2277. https://doi.org/10.1101/gad.1670908.

Hartl, F.U., Bracher, A., and Hayer-Hartl, M. (2011). Molecular chaperones in protein folding and proteostasis. Nature *475*, 324–332. https://doi.org/10.1038/nature10317.

Hartl, F.U., and Hayer-Hartl, M. (2009). Converging concepts of protein folding in vitro and in vivo. Nat. Struct. Mol. Biol. *16*, 574–581. https://doi.org/10.1038/nsmb.1591.

Hingorani, K.S., Metcalf, M.C., Deming, D.T., Garman, S.C., Powers, E.T., and Gierasch, L.M. (2017). Ligand-promoted protein folding by biased kinetic partitioning. Nat. Chem. Biol. *13*, 369–371. https://doi.org/10.1038/nchembio.2303.

Hvidt, A., and Nielsen, S.O. (1966). Hydrogen exchange in proteins. Adv. Protein Chem. *21*, 287–386. https://doi.org/10.1016/s0065-3233(08)60129-1.

Johansson, K.E., Mashahreh, B., Hartmann-Petersen, R., Ravid, T., and Lindorff-Larsen, K. (2022). Prediction of quality-control degradation signals in yeast proteins. Preprint at bioRxiv. https://doi.org/10.1101/2022.04.06.487301.

Kampmeyer, C., Karakostova, A., Schenstrom, S.M., Abildgaard, A.B., Lauridsen, A.M., Jourdain, I., and Hartmann-Petersen, R. (2017). The exocyst subunit Sec3 is regulated by a protein quality control pathway. J. Biol. Chem. *292*, 15240–15253. https://doi.org/10.1074/jbc.m117.789867.

Kandasamy, G., and Andreasson, C. (2018). Hsp70-Hsp110 chaperones deliver ubiquitin-dependent and -independent substrates to the 26S proteasome for proteolysis in yeast. J. Cell Sci. *131*, jcs210948. https://doi.org/10.1242/jcs.210948.

Kazimierczuk, K., and Orekhov, V.Y. (2011). Accelerated NMR spectroscopy by using compressed sensing. Angew. Chem. Int. Ed. Engl. *123*, 5670–5673. https://doi.org/10.1002/ange.201100370.

Kim, Y.E., Hipp, M.S., Bracher, A., Hayer-Hartl, M., and Ulrich Hartl, F. (2013). Molecular chaperone functions in protein folding and proteostasis. Annu. Rev. Biochem. *82*, 323–355. https://doi.org/10.1146/annurev-biochem-060208-092442.

Koren, I., Timms, R.T., Kula, T., Xu, Q., Li, M.Z., and Elledge, S.J. (2018). The eukaryotic proteome is shaped by E3 Ubiquitin ligases targeting C-terminal degrons. Cell *173*, 1622–1635.e14. https://doi.org/10.1016/j.cell.2018.04.028.

Kriegenburg, F., Jakopec, V., Poulsen, E.G., Nielsen, S.V., Roguev, A., Krogan, N., Gordon, C., Fleig, U., and Hartmann-Petersen, R. (2014). A chaperone-assisted degradation pathway targets kinetochore proteins to ensure genome stability. PLoS Genet. *10*, e1004140. https://doi.org/10.1371/journal.pgen.1004140.

Mashahreh, B., Armony, S., Johansson, K.E., Chapelbaum, A., Friedman, N., Gardner, R.G., Hartmann-Petersen, R., Lindorff-Larsen, K., and Ravid, T. (2022). Conserved degronome features governing quality control-associated proteolysis. Preprint at bioRxiv. https://doi.org/10.1101/2022.04.06.487275.

Mathiassen, S.G., Larsen, I.B., Poulsen, E.G., Madsen, C.T., Papaleo, E., Lindorff-Larsen, K., Kragelund, B.B., Nielsen, M.L., Kriegenburg, F., and Hartmann-Petersen, R. (2015). A two-step protein quality control pathway for a misfolded DJ-1 variant in fission yeast. J. Biol. Chem. *290*, 21141–21153. https://doi.org/10.1074/jbc.m115.662312.

Matreyek, K.A., Starita, L.M., Stephany, J.J., Martin, B., Chiasson, M.A., Gray, V.E., Kircher, M., Khechaduri, A., Dines, J.N., Hause, R.J., et al. (2018). Multiplex assessment of protein variant abundance by massively parallel sequencing. Nat. Genet. *50*, 874–882. https://doi.org/10.1038/s41588-018-0122-z.

Maurer, M.J., Spear, E.D., Yu, A.T., Lee, E.J., Shahzad, S., and Michaelis, S. (2016). Degradation signals for ubiquitin-proteasome dependent cytosolic protein quality control (CytoQC) in yeast. G3. (Bethesda.). *6*, 1853–1866. https://doi.org/10.1534/g3.116.027953.

Maxwell, K.L., Wildes, D., Zarrine-Afsar, A., De Los Rios, M.A., Brown, A.G., Friel, C.T., Hedberg, L., Horng, J.C., Bona, D., Miller, E.J., et al. (2005). Protein folding: defining a "standard" set of experimental conditions and a preliminary kinetic data set of two-state proteins. Protein Sci. *14*, 602–616. https://doi.org/10.1110/ps.041205405.

Metzger, M.B., Maurer, M.J., Dancy, B.M., and Michaelis, S. (2008). Degradation of a cytosolic protein requires endoplasmic reticulum-associated degradation machinery. J. Biol. Chem. *283*, 32302–32316. https://doi.org/10.1074/jbc.m806424200.

Murata, S., Minami, Y., Minami, M., Chiba, T., and Tanaka, K. (2001). CHIP is a chaperone-dependent E3 ligase that ubiquitylates unfolded protein. EMBO Rep. *2*, 1133–1138. https://doi.org/10.1093/embo-reports/kve246.

Pey, A.L., Stricher, F., Serrano, L., and Martinez, A. (2007). Predicted effects of missense mutations on native-state stability account for phenotypic outcome in phenylketonuria, a paradigm of misfolding diseases. Am. J. Hum. Genet. *81*, 1006–1024. https://doi.org/10.1086/521879.

Polshakov, V.I., Birdsall, B., and Feeney, J. (2006). Effects of co-operative ligand binding on protein amide NH hydrogen exchange. J. Mol. Biol. *356*, 886–903. https://doi.org/10.1016/j.jmb.2005.11.084.

Qian, S.B., McDonough, H., Boellmann, F., Cyr, D.M., and Patterson, C. (2006). CHIP-mediated stress recovery by sequential ubiquitination of substrates and Hsp70. Nature *440*, 551–555. https://doi.org/10.1038/nature04600.

Ravid, T., and Hochstrasser, M. (2008). Diversity of degradation signals in the ubiquitin-proteasome system. Nat. Rev. Mol. Cell Biol. *9*, 679–689. https://doi.org/10.1038/nrm2468.

Ravid, T., Kreft, S.G., and Hochstrasser, M. (2006). Membrane and soluble substrates of the Doa10 ubiquitin ligase are degraded by distinct pathways. EMBO J. *25*, 533–543. https://doi.org/10.1038/sj.emboj.7600946.

Rosenbaum, J.C., Fredrickson, E.K., Oeser, M.L., Garrett-Engele, C.M., Locke, M.N., Richardson, L.A., Nelson, Z.W., Hetrick, E.D., Milac, T.I., Gottschling, D.E., and Gardner, R.G. (2011). Disorder targets misorder in nuclear quality control degradation: a disordered ubiquitin ligase directly recognizes its misfolded substrates. Mol. Cell *41*, 93–106. https://doi.org/10.1016/j.molcel.2010.12.004.

Rudiger, S., Buchberger, A., and Bukau, B. (1997). Interaction of Hsp70 chaperones with substrates. Nat. Struct. Biol. *4*, 342–349. https://doi.org/10.1038/nsb0597-342.

Samant, R.S., Livingston, C.M., Sontag, E.M., and Frydman, J. (2018). Distinct proteostasis circuits cooperate in nuclear and cytoplasmic protein quality control. Nature *563*, 407–411. https://doi.org/10.1038/s41586-018-0678-x.

Scheller, R., Stein, A., Nielsen, S.V., Marin, F.I., Gerdes, A.M., Marco, M., Di, M.M., Papaleo, E., Lindorff-Larsen, K., and Hartmann-Petersen, R. (2019). Toward mechanistic models for genotype-phenotype correlations in phenylketonuria using protein stability calculations. Hum. Mutat. *40*, 444–457. https://doi.org/10.1002/humu.23707.

Shiber, A., and Ravid, T. (2014). Chaperoning proteins for destruction: diverse roles of Hsp70 chaperones and their co-chaperones in targeting misfolded proteins to the proteasome. Biomolecules *4*, 704–724. https://doi.org/10.3390/biom4030704.

Skinner, S.P., Fogh, R.H., Boucher, W., Ragan, T.J., Mureddu, L.G., and Vuister, G.W. (2016). CcpNmr AnalysisAssign: a flexible platform for integrated NMR analysis. J. Biomol. NMR *66*, 111–124. https://doi.org/10.1007/s10858-016-0060-y.

Stein, A., Fowler, D.M., Hartmann-Petersen, R., and Lindorff-Larsen, K. (2019). Biophysical and mechanistic models for disease-causing protein variants. Trends Biochem. Sci. *44*, 575–588. https://doi.org/10.1016/j.tibs.2019.01.003.

Thompson, S., Zhang, Y., Ingle, C., Reynolds, K.A., and Kortemme, T. (2020). Altered expression of a quality control protease in E. coli reshapes the in vivo mutational landscape of a model enzyme. Elife *9*, e53476. https://doi.org/10.7554/elife.53476.

Timms, R.T., Zhang, Z., Rhee, D.Y., Harper, J.W., Koren, I., and Elledge, S.J. (2019). A glycine-specific N-degron pathway mediates the quality control of protein N-myristoylation. Science *365*, eaaw4912. https://doi.org/10.1126/science.aaw4912.

van der Lee, R., Lang, B., Kruse, K., Gsponer, J., Sánchez de Groot, N., Huynen, M.A., Matouschek, A., Fuxreiter, M., and Babu, M.M. (2014). Intrinsically disordered segments affect protein half-life in the cell and during evolution. Cell Rep. *8*, 1832–1844. https://doi.org/10.1016/j.celrep.2014.07.055.

Watson, M.D., Monroe, J., and Raleigh, D.P. (2018). Size-dependent relationships between protein stability and thermal unfolding temperature have important implications for analysis of protein energetics and high-throughput assays of protein-ligand interactions. J. Phys. Chem. B *122*, 5278–5285. https://doi.org/10.1021/acs.jpcb.7b05684.

Xu, W., Marcu, M., Yuan, X., Mimnaugh, E., Patterson, C., and Neckers, L. (2002). Chaperone-dependent E3 ubiquitin ligase CHIP mediates a degradative pathway for c-ErbB2/Neu. Proc. Natl. Acad. Sci. U. S. A *99*, 12847–12852. https://doi.org/10.1073/pnas.202365899.

Yamamoto, T., Izumi, S., and Gekko, K. (2004). Mass spectrometry on hydrogen/deuterium exchange of dihydrofolate reductase: effects of ligand binding. J. Biochem. *135*, 663–671. https://doi.org/10.1093/jb/mvh080.

Yin, Y., and Moult, J. (2019). Characterizing and comparing missense variants in monogenic disease and in cancer. Preprint at bioRxiv. https://doi.org/10.1101/534693.

Yuan, Z. (2005). Better prediction of protein contact number using a support vector regression analysis of amino acid sequence. BMC Bioinf. *6*, 248. https://doi.org/10.1186/1471-2105-6-248.

Please cite this article in press as: Kampmeyer et al., Disease-linked mutations cause exposure of a protein quality control degron, Structure (2022), https://doi.org/10.1016/j.str.2022.05.016

STAR★METHODS

KEY RESOURCES TABLE

REAGENT or RESOURCE	SOURCE	IDENTIFIER
Antibodies		
Polyclonal anti-DHFR antibody produced in rabbit	ProteinTech	Cat# 15194-1-AP; RRID: AB_209158
Monoclonal anti-HA antibody produced in rat	Roche	Cat# 3F10; RRID: AB_2314622
Monoclonal anti-alpha-Tubulin produced in mouse	Sigma-Aldrich	Cat# 00020911; RRID: AB_10013740
Monoclonal anti-Pma1 produced in mouse	Abcam	Cat# ab4645; RRID: AB_30455
Monoclonal anti-Myc produced in rat	ChromoTek	Cat# 9e1-100; RRID: AB_2631398
Goat anti-Mouse IgG, HRP conjugate	Dako/Agilent	Cat# P0447; RRID: AB_261713
Swine anti-Rabbit IgG, HRP conjugate	Dako/Agilent	Agilent Cat# P0217; RRID: AB_2728719
Goat anti-Rat IgG, HRP conjugate	Thermo Fisher Scientific	Cat# 31470; RRID: AB_228356
Chemicals, peptides, and recombinant proteins		
Bortezomib	LC Laboratories	Cat# B-1408
Methotrexate	Sigma-Aldrich	Cat# M8407
Folate	Sigma-Aldrich	Cat# F7876
Methotrexate-agarose	Sigma-Aldrich	Cat# M0269
$^{15}NH_4Cl$	CortecNet	Cat# CN80P10,
^{13}C-glucose	CortecNet	Cat# CC860P10
IPTG, isopropyl-beta-D-thiogalactoside	Invitrogen	Cat# AM9464
Complete protease inhibitor tablets without EDTA	Roche	Cat# 04693132001
PMSF, phenylmethylsulfonyl fluoride	Thermo Fisher Scientific	Cat# 36978
TALON metal affinity resin	Clontech	Cat# 635502
SUMO protease, His-tagged	Sigma-Aldrich	Cat# SAE0067
Critical commercial assays		
BCA protein assay kit	Pierce	Cat# 23225
Deposited data		
DHFR wild-type	This paper	BMRB ID: 51192
DHFR L80F	This paper	BMRB ID: 51194
DHFR D153V	This paper	BMRB ID: 51195
Experimental models: Organisms/strains		
E. coli TOP10 competent cells	Thermo Fisher Scientific	Cat# C404010
E. coli BL21(DE3) pLysS competent cells	Thermo Fisher Scientific	Cat# C606010
Yeast *S. cerevisiae* wild-type, MatA, *his3Δ1*, *leu2Δ0*, *met15Δ0*, *ura3Δ0*	Invitrogen	Cat# 95401.H2
Yeast *S. cerevisiae ssa1*Δ, MatA, *his3Δ1*, *leu2Δ0*, *met15Δ0*, *ura3Δ0*, *ssa1*::*KanMX*	Invitrogen	Cat# 95401.H2
Yeast *S. cerevisiae ssa2*Δ, MatA, *his3Δ1*, *leu2Δ0*, *met15Δ0*, *ura3Δ0*, *ssa2*::*KanMX*	Invitrogen	Cat# 95401.H2
Recombinant DNA		
pTR1412-Ura3-HA-GFP-(vector control)	(Geffen et al., 2016)	N/A
pTR1412-Ura3-HA-GFP-CL1	(Geffen et al., 2016)	N/A
pTR1412 (vector control)	This paper	N/A
pTR1412-DHFR wt	This paper	N/A
pTR1412-DHFR L80F	This paper	N/A
pTR1412-DHFR D153V	This paper	N/A
pTR1412-DHFR L80F, N73A	This paper	N/A
pTR1412-DHFR L80F, K69E	This paper	N/A
pTR1412-DHFR L80F, R78E	This paper	N/A

(*Continued on next page*)

Please cite this article in press as: Kampmeyer et al., Disease-linked mutations cause exposure of a protein quality control degron, Structure (2022), https://doi.org/10.1016/j.str.2022.05.016

Continued

REAGENT or RESOURCE	SOURCE	IDENTIFIER
pTR1412-DHFR L80F, K69E, R78E	This paper	N/A
pTR1412-Ura3-HA-GFP-DHFR 1-24	This paper	N/A
pTR1412-Ura3-HA-GFP-DHFR 13-36	This paper	N/A
pTR1412-Ura3-HA-GFP-DHFR 25-48	This paper	N/A
pTR1412-Ura3-HA-GFP-DHFR 37-60	This paper	N/A
pTR1412-Ura3-HA-GFP-DHFR 49-72	This paper	N/A
pTR1412-Ura3-HA-GFP-DHFR 61-84	This paper	N/A
pTR1412-Ura3-HA-GFP-DHFR 73-96	This paper	N/A
pTR1412-Ura3-HA-GFP-DHFR 85-108	This paper	N/A
pTR1412-Ura3-HA-GFP-DHFR 97-120	This paper	N/A
pTR1412-Ura3-HA-GFP-DHFR 109-132	This paper	N/A
pTR1412-Ura3-HA-GFP-DHFR 121-144	This paper	N/A
pTR1412-Ura3-HA-GFP-DHFR 133-156	This paper	N/A
pTR1412-Ura3-HA-GFP-DHFR 145-168	This paper	N/A
pTR1412-Ura3-HA-GFP-DHFR 157-180	This paper	N/A
pTR1412-Ura3-HA-GFP-DHFR 164-187	This paper	N/A
pTR1412-Ura3-HA-GFP-DHFR Deg1 Φ0	This paper	N/A
pTR1412-Ura3-HA-GFP-DHFR Deg2 Φ0	This paper	N/A
pTR1412-Ura3-HA-GFP-DHFR Deg1 K-all-R	This paper	N/A
pTR1412-Ura3-HA-GFP-DHFR Deg2 K-all-R	This paper	N/A
pTR1412-Ura3-HA-GFP-DHFR Deg2 L80F	This paper	N/A
pTR1412-Ura3-HA-GFP-DHFR Deg2 Δ8	This paper	N/A
pTR1412-Ura3-HA-GFP-DHFR Deg2 Δ12	This paper	N/A
pTR1412-Ura3-HA-GFP-DHFR Deg2 Δ16	This paper	N/A
pTR1412-Ura3-HA-GFP-DHFR Deg2 Δ18	This paper	N/A
pTR1412-Ura3-HA-GFP-DHFR Deg2 Δ20	This paper	N/A
pESC-myc-DHFR wt	This paper	N/A
pESC-myc-DHFR L80F	This paper	N/A
pESC-myc-DHFR D153V	This paper	N/A
pET28a-6His-SUMO1-DHFR wt	This paper	N/A
pET28a-6His-SUMO1-DHFR L80F	This paper	N/A
pET28a-6His-SUMO1-DHFR D153V	This paper	N/A
Software and algorithms		
PyMOL	Schrodinger	Version 2.3
nmrPipe	(Delaglio et al., 1995)	http://www.ibbr.umd.edu/nmrpipe/
qMDD	(Kazimierczuk and Orekhov, 2011)	http://mddnmr.spektrino.com
CCPNMR analysis	(Skinner et al., 2016)	https://www.ccpn.ac.uk/v2-software/software/analysis
Other		
Nanotemper Prometheus	Nanotemper	Model NT.48
Mini-Beadbeater-16	BioSpec Products Inc.	Model 16, Cat#607
Microplate reader	Tecan	Model Infinite 200 Pro

RESOURCE AVAILABILITY

Lead contact

Further information and requests for resources should be directed to and will be fulfilled by the lead contact, Rasmus Hartmann-Petersen (rhpetersen@bio.ku.dk).

Materials availability

Plasmids generated in this study may be requested from the lead contact.

Please cite this article in press as: Kampmeyer et al., Disease-linked mutations cause exposure of a protein quality control degron, Structure (2022), https://doi.org/10.1016/j.str.2022.05.016

Data and code availability

- The NMR data have been deposited at the Biological Magnetic Resonance Data Bank and are publicly available as of the date of publication. Accession numbers are listed in the key resources table.
- This paper does not report original code.
- Any additional information required to reanalyze the data reported in this paper is available from the lead contact upon request.

EXPERIMENTAL MODEL AND SUBJECT DETAILS

Plasmid DNA was amplified in *Escherichia coli* TOP10 cells in Lysogeny broth (LB) at 37°C.

Recombinant proteins were expressed in *Escherichia coli* BL21(DE3) pLysS in M9 minimal media supplemented with 2 mM folic acid at 37°C. The cells were induced at OD_{600nm} 0.5 for 16-18 hours at 15°C with 0.5 mM IPTG.

Saccharomyces cerevisiae yeast strains (see Key resource table) were cultured in synthetic complete (SC) medium (2% glucose, 6.7 g/L yeast nitrogen base without amino acids and with ammonium sulfate (Sigma)) supplemented with 1.92 g/L Drop-out Mix Synthetic (US Biological) as required for selection.

METHOD DETAILS

Cloning

Human *DHFR* cDNA fragments were inserted into the pTR1412 vector (Geffen et al., 2016) in frame after the *URA3-HA-GFP* fusion (Genscript). Full-length *DHFR* was expressed in yeast from pTR1412 lacking the *URA3-HA-GFP* fusion (Genscript) or from pESC (Genscript). Point mutations were generated by Genscript. For production of DHFR and DHFR variants in *E. coli*, codon optimized human DHFR was produced as a 6His-SUMO1 fusion from pET28a (Genscript). All plasmids are listed in the Key resource table.

Yeast strains and techniques

Yeast cells were transformed using lithium acetate (Gietz and Schiestl, 2007). Briefly, 50 mL of $2x10^7$ cells/mL in exponential phase were harvested and washed in sterile water by centrifugation (3000 g, 5 min) before 0.1 mL containing 10^8 cells was added to 360 μL of a transformation mix composed of: 240 μL 50% PEG-3350 (Sigma), 36 μL 1 M LiAc (Sigma), 50 μL 2 mg/mL freshly denatured salmon sperm DNA (Sigma) in TE (10 mM Tris/HCl, 1 mM EDTA, pH 8), and 34 μL diluted plasmid DNA. After 40 minutes incubation at 42°C, the cells were harvested by centrifugation (13000 g, 1 min.), resuspended in sterile water and plated. For solid media growth assays, the strains were cultured at 30°C to exponential phase. The cultures were diluted to an OD_{600nm} of exactly 0.40 and dilution series (5-fold) were prepared. Then, 5 μL of each dilution was applied in drops on agar plates. Colonies formed after 2-3 days incubation at 30°C. In growth assays, Bortezomib (LC laboratories) was used at a final concentration of 0.5 mM. For liquid media growth assays, pre-cultures were diluted to an OD_{600nm} of 0.01 and added to a 96-well plate with a cover (Nunc) in triplicates. Wells only containing media, were included as a reference. Turbidity of the cultures was monitored as OD_{600nm} in an Infinite 200 PRO (Tecan) microplate reader for 24 hours at 30°C. The growth curves were used for estimating the doubling times. For SDS-PAGE and western blotting of the degron-fusions, cell lysates were prepared from exponential phase cultures treated with 0.1 mM $CuSO_4$ overnight to induce expression. The full-length DHFR variants were produced without $CuSO_4$. Bortezomib (LC laboratories) was used at a final concentration of 1 mM and methotrexate at a final concentration of 250 μM. The cells were lysed using glass beads and trichloroacetic acid (TCA) based on a previous procedure (Cox et al., 1997). Briefly, $1.2x10^8$ cells in exponential phase were harvested and washed in water by centrifugation (3000 g, 5 min). The cells were resuspended in 1 mL of 20% trichloroacetic acid (TCA) and centrifuged (3000 g, 5 min). The pellet was resuspended in 200 μL of 20% TCA and transferred to 2 mL screwcap tubes with 0.5 mL 400-600 micron glass beads (Sigma). The tubes were inserted into a Mini-BeadBeater machine (BioSpec Products Inc.) and 3 cycles of 10 sec were applied. Then, 400 μL 5% TCA was added and the material was eluted by centrifugation (1000 g, 5 min) through a hole punched through the bottom of the tube with a needle. The eluted material was centrifuged (10000 g, 5 min.) at 4°C and the pellet washed with 80% ice-cold acetone. Finally, the pellet was resuspended in 0.1 mL SDS sample buffer (62.5 mM Tris/HCl pH 6.8, 2% SDS, 25% glycerol, 0.01% bromphenol blue, 5% β-mercaptoethanol). For microscopy, live cells in exponential phase were imaged using a Zeiss Axio Imager Z1 microscope equipped with a Hamamatsu ORCA-ER digital camera.

Solubility and co-precipitation experiments

Protein solubility was analyzed from yeast cells in exponential phase. Cell lysates were prepared using glass beads in buffer A (25 mM Tris/HCl pH 7.4, 50 mM NaCl, 10% glycerol, 2 mM $MgCl_2$, 1 mM PMSF and Complete Mini Protease Inhibitors (Roche)) with 3 × 10 sec cycles on a Mini-BeadBeater machine (BioSpec Products Inc.). The whole cell lysates were centrifuged (13000 g, 30 min.) to separate the soluble and insoluble proteins. The pellet was resuspended in a volume of buffer A matching the volume of the supernatant, then SDS sample buffer was added and the samples were analyzed by SDS-PAGE and Western blotting.

Co-precipitation experiments were performed from exponential phase cultures treated with 0.1 mM $CuSO_4$ overnight to induce expression. Cells were lysed using glass beads in 1 cell volume of buffer B (20 mM Tris/HCl pH 7.4, 1 mM EDTA, 1 mM DTT, 10% glycerol, 1 mM PMSF and Complete protease inhibitors (Roche)) with 3 × 10 sec cycles on a Mini-BeadBeater machine (BioSpec Products Inc.). The extracts were cleared by centrifugation (13000 g, 30 min.), and the soluble fraction tumbled

Please cite this article in press as: Kampmeyer et al., Disease-linked mutations cause exposure of a protein quality control degron, Structure (2022), https://doi.org/10.1016/j.str.2022.05.016

end-over-end for 2 hours with 15 μL (bed volume) of methotrexate-agarose (Sigma). Then the beads were washed once in 1 mL of buffer B with 0.5 M KCl, three times with buffer B containing 0.5 M KCl and 1% Triton X-100, and finally once in buffer B with 0.5 M KCl. Protein was eluted in buffer B with 0.5 M KCl and 1 mM methotrexate (Sigma). Then the protein was precipitated with 40% TCA for 60 minutes on ice followed by centrifugation (10000 g, 30 min.). The pellets were extensively washed with ice-cold acetone and air-dried. Finally, the pellets were resuspended in SDS sample buffer and analyzed by SDS-PAGE and Western blotting.

Electrophoresis and blotting

For SDS-PAGE and Western blotting, protein samples were resolved on 12.5% acrylamide gels and transferred to 0.2 μm nitrocellulose membranes by electro-blotting. Blocking was performed in PBS (10 mM Na_2HPO_4, 1.8 mM KH_2PO_4, 137 mM NaCl, 3 mM KCl, pH 7.4) with 5% milk powder. The antibodies used are listed in the Key resource table. An independent repeat of the shown blots is included in the supplemental material (Figure S4).

In silico methods

Protein structures were visualized using PyMOL version 2.3 and the DHFR structure (PDB: 1U72) (Cody et al., 2005). C-beta neighbors were calculated based on the coordinates of PDB 1U72. For each residue, we calculated the number of C-beta atoms within 8 Å of its C-beta (C-alpha for glycine) and set this as the number of C-beta neighbors. Residues with >10 C-beta neighbors are considered buried, while those with fewer C-beta neighbors are considered exposed (Yuan, 2005).

Purification of DHFR variants, expressed in *E. coli*

The DHFR variants were produced in *E. coli* BL21(DE3) pLysS from a pET28a(+)-based plasmid fused N-terminally to a 6His-SUMO tag. Overnight cultures were diluted 200-fold in 1 L M9 minimal media supplemented with 2 mM folic acid, kanamycin and chloramphenicol, and incubated at 37°C. For single and double-labelled protein production, the NH_4Cl and glucose content of the M9 minimal media were replaced with $^{15}NH_4Cl$ (CortecNet) and/or ^{13}C-glucose (CortecNet), respectively. When OD_{600nm} reached 0.5, the cultures were moved to 15°C for 30 minutes before addition of IPTG to 0.5 mM. After 16-18 hours the cells were harvested by centrifugation. The cell pellet was resuspended in 40 mL lysis buffer (50 mM NaH_2PO_4 pH 7.4, 300 mM NaCl, 1 mM PMSF and Complete protease inhibitors without EDTA (Roche)) and sonicated on ice. The lysate was cleared by centrifugation (13000 g, 30 min) and the supernatant passed over a 1 mL column packed with TALON resin (Clontech). The column was washed with 30 mL lysis buffer and 10 mL lysis buffer containing 10 mM imidazole. Elution was performed with lysis buffer containing 250 mM imidazole. Fractions containing the DHFR protein were pooled and dialyzed against cleavage buffer (25 mM Na-phosphate pH 7.4, 150 mM NaCl, 0.5 mM folate) overnight at 4°C. The following day, DTT was added to a final concentration of 0.5 mM and His-SUMO protease (Sigma) was added to a concentration 100-fold lower than the total protein concentration. After 2 hours at 4°C the reaction mixture was passed over a second TALON resin column, and the cleaved DHFR was collected as flow-through. Pooled fractions were dialyzed overnight against NMR buffer (50 mM K-phosphate pH 6.5, 100 mM KCl, 1 mM DTT, 25 μM folic acid). By SDS-PAGE analysis the purified proteins were estimated to be >95% pure. The protein concentration was determined by a bicinchoninic acid (BCA) assay (Pierce) using bovine serum albumin (BSA) as a standard. The yield was roughly 20-30 mg of DHFR from 1 L of M9 culture.

Heat denaturation

Samples of 25 μM of each DHFR variant were prepared by dilution in 50 mM K-phosphate, 100 mM KCl, 1 mM DTT, 25 μM folate, pH 6.5. To replace bound folate, 50 μM MTX was added to the folate samples. The unfolding of DHFR was followed by intrinsic Trp fluorescence using a Nanotemper Prometheus NT.48 fluorimeter. Samples of 15 μL were placed in high sensitivity quarts capillaries (Nanotemper) and the temperature was ramped with 1°C/min from 20°C to 95°C. The fluorescence signal at 350 nm was normalized to represent the fraction of unfolded protein.

Chemical shift assignments

^{13}C-^{15}N double labelled samples of all variants were prepared with a protein concentration of 300 μM in 50 mM K-phosphate, 100 mM KCl, 1 mM DTT, 25 μM folate, pH 6.5. ^{15}N-HSQC, HNCO, HNCA, HNCOCA, HNCOCACB and HNCACB were recorded on a 800 MHz Bruker Avance III spectrometer at 25°C. The triple resonance spectra were recorded with 25% non-uniform sampling and reconstructed by compressed sensing using the iterative soft threshold algorithm with virtual echo implemented in qMDD (Kazimierczuk and Orekhov, 2011) and processed using nmrPipe (Delaglio et al., 1995). Backbone H^N, $^{15}N^H$, $^{13}C'$, $^{13}C\alpha$ and $^{13}C\beta$ chemical shifts were assigned using ccpnmr analysis (Skinner et al., 2016) and the previously published assignment of wild-type DHFR (Bhabha et al., 2013).

Hydrogen-deuterium exchange

To measure the hydrogen exchange in D_2O, 600 μL of 400 μM ^{15}N-labelled protein in 50 mM K-phosphate, 50 mM KCl, 1 mM DTT, 25 μM folate, pH 6.5 were lyophilized, and the resulting protein powder resuspended in 600 μL cold 99.9% D_2O. The HDX time series of all three variants were recorded on a 750 MHz Bruker Advance III HD spectrometer at 25°C using a standard HSQC pulse program. The acquisition time for each experiment was 19.53 minutes and 275 HSQC were recorded for each variant corresponding to 91.5 hours.

Please cite this article in press as: Kampmeyer et al., Disease-linked mutations cause exposure of a protein quality control degron, Structure (2022), https://doi.org/10.1016/j.str.2022.05.016

The spectra were processed, and peaks intensities measured with nmrPipe (Delaglio et al., 1995). For each peak, the data was fitted to a single exponential decay with an offset, $I(t) = (I_o - I_\infty)*\exp(-k*t) + I_\infty$ (Hvidt and Nielsen, 1966). For amides where the exchange reached a final plateau in all three variants, I_∞ was fitted as a global parameter for all three variants. For residues where a plateau was not reached, the data were fitted with I_∞ fixed at the average value from the residues where this parameter could be estimated.

QUANTIFICATION AND STATISTICAL ANALYSIS

The doubling times for the liquid growth assays were performed in triplicates. The individual data points, means and standard deviations are presented. No statistical tests were employed.